Gerrit J. Jager, MD • Emiel T. G. Ruijter, MD • Christina A. vd Kaa, MD
Jean J. M. C. H. de la Rosette, MD, PhD • Gosse O. N. Oosterhof, MD, PhD
John R. Thornbury, MD • Sjef H. J. Ruijs, MD, PhD • Jelle O. Barentsz, MD, PhD

Dynamic TurboFLASH Subtraction Technique for Contrast-enhanced MR Imaging of the Prostate: Correlation with Histopathologic Results[1]

PURPOSE: **To assess whether a TurboFLASH (fast low-angle shot) magnetic resonance (MR) sequence can improve the accuracy of fast spin-echo (SE) endorectal coil MR imaging in the staging and localization of prostate cancer.**

MATERIALS AND METHODS: **In 57 patients with prostate cancer, MR imaging was performed with the following sequences: T1-weighted SE, T2-weighted fast SE, single-section gadolinium-enhanced dynamic subtracted TurboFLASH (one image every 1.25 or 2.5 seconds), and late-phase gadolinium-enhanced T1-weighted SE. Retrospectively, two blinded independent readers graded onset and steepest slope of enhancement and assessed tumor involvement and capsular penetration. MR findings were correlated with histopathologic results.**

RESULTS: **On TurboFLASH images, prostate cancer was characterized by early and rapidly accelerating enhancement compared with that of surrounding tissues. Average sensitivity, specificity, and accuracy for detection of tumor involvement for the two readers with TurboFLASH images were 73.5%, 81.0%, and 77.5%. These values with fast SE images were 57.5%, 80.5%, and 72.0%. Depiction of capsular penetration and delineation and staging of tumor were better when TurboFLASH images were included with fast SE images. Differences between the two sequences, however, were not statistically significant.**

CONCLUSION: **Because the TurboFLASH sequence did not statistically significantly improve tumor localization and staging results, routine use is not recommended. The technique may be useful for selected patients with equivocal evidence of capsular penetration.**

MAGNETIC resonance (MR) imaging is considered an effective tool for staging prostate cancer (1). The information obtained with this modality, however, adds little to the information obtained by the traditional means of clinical staging and biopsy, such as tumor grade, number and length of cores containing malignancy, and involvement of seminal vesicles (2–4).

The use of a gadolinium chelate to increase the diagnostic information of MR imaging has been described in the literature (5–10). The results of these studies suggest that contrast material–enhanced T1-weighted MR imaging does not provide additional information compared with that obtained from T2-weighted imaging, but that the T1-weighted sequence may be useful in evaluating seminal vesicle invasion in equivocal cases (6,10). Therefore, the use of a gadolinium chelate is not warranted for routine staging of prostate cancer. Brown et al (8) evaluated early-phase, T1-weighted, bolus-enhanced MR imaging for the evaluation of prostate cancer. They found that the information provided by T1-weighted images during the early phase of contrast enhancement enables the best delineation of tumor within the gland.

Experience with dynamic subtraction TurboFLASH ([fast low-angle shot] Siemens, Erlangen, Germany) MR imaging in bladder and breast cancer indicates that malignant lesions demonstrate an earlier and faster enhancement compared with that of benign lesions (11,12). To our knowledge, the diagnostic value of fast dynamic contrast enhancement in prostate cancer has not been evaluated previously. The aim of the present study was to evaluate the complementary diagnostic value of single-section dynamic subtraction TurboFLASH MR imaging in patients with prostate cancer.

MATERIALS AND METHODS

The patient population comprised 57 men (age range, 48–73 years; mean age, 64 years) with clinically localized prostate cancer who underwent dynamic subtraction TurboFLASH MR imaging complementary to the routine staging MR examination of the prostate. The examinations were performed between August 1993 and February 1996. Only patients who underwent radical prostatectomy were included in this study. Patients who received hormonal treatment before surgery were excluded from this study. Biopsy procedures preceded MR imaging by an average of 3 weeks. Patients underwent radical prostatectomy within 3 weeks after imaging. All prostatectomy procedures were performed in patients in whom no lymph node metastases were found at laparoscopic lymph node dissection before the operation or at frozen section examination during the operation.

MR Technique

All images were obtained with a commercially available 1.5-T MR system (Magnetom SP; Siemens) by using an endorec-

Index terms: Gadolinium • Magnetic resonance (MR), pulse sequences, 844. 121411, 844.121416, 844.12143 • Prostate, MR, 844.121411, 844.121416 • Prostate, neoplasms, 844.32 • Prostate, surgery, 844.451

Abbreviations: BPH = benign prostatic hyperplasia, FLASH = fast low-angle shot, SE = spin echo.

Radiology 1997; 203:645–652

[1] From the Departments of Radiology (G.J.J., S.H.J.R., J.O.B.), Urology (E.T.G.R., J.J.M.C.H.d.l.R, G.O.N.O.), and Pathology (E.T.G.R., C.A.vd.K.), University Hospital Nijmegen, 6500 NB, Nijmegen, The Netherlands; and the Department of Radiology, University of Wisconsin, Madison (J.R.T.). From the 1996 RSNA scientific assembly. Received September 19, 1996; revision requested October 24; revision received February 6, 1997; accepted February 18. **Address reprint requests to** G.J.J.

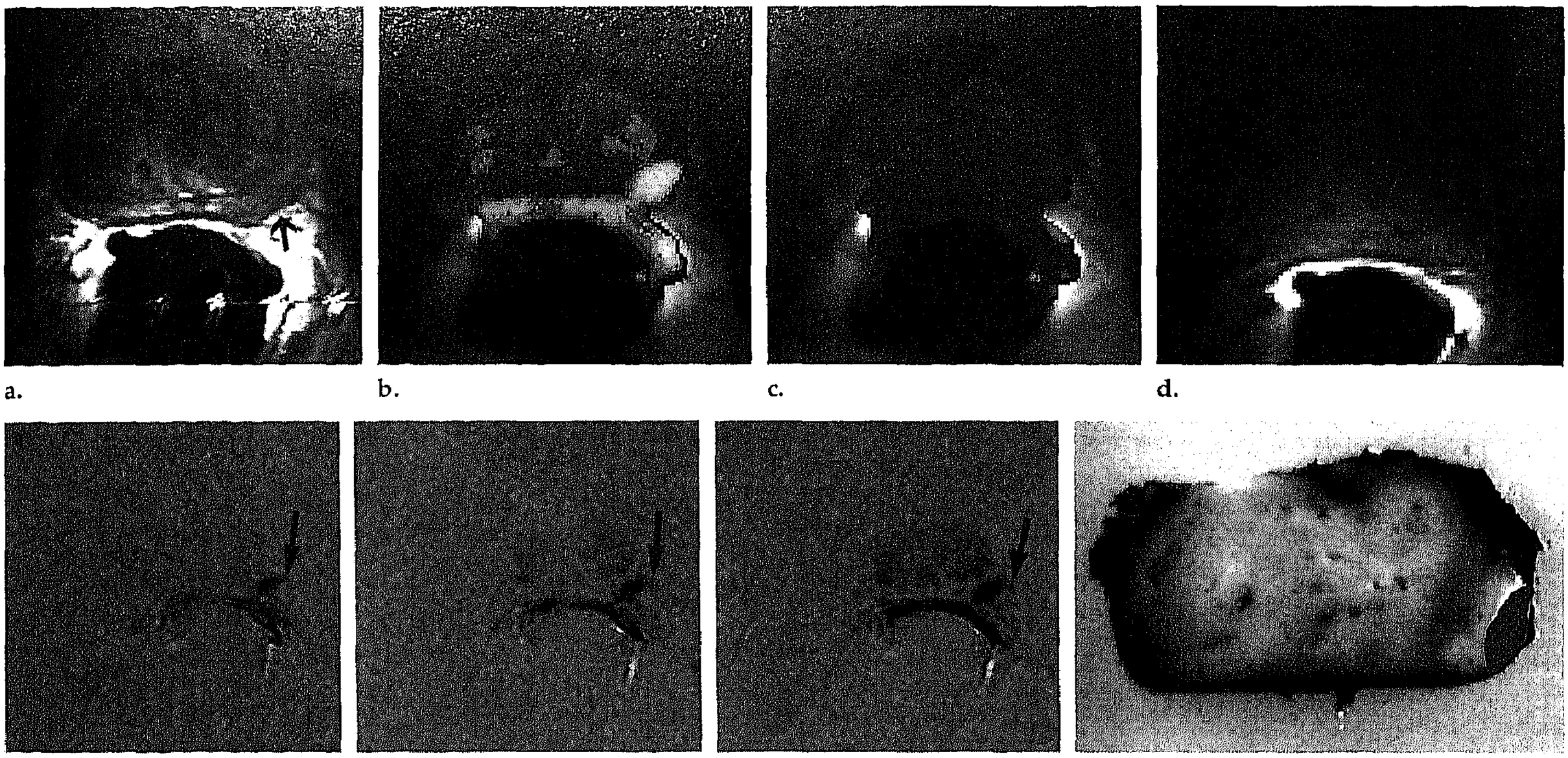

Figure 1. Case of a 63-year-old man with a poorly differentiated tumor on the left side. **(a)** Fast SE image shows a small low-signal-intensity area in the peripheral zone on the left side (arrow). **(b)** Time image shows very early and rapid enhancement. **(c)** Negative slope image shows a relatively high washout. **(d)** Postcontrast T1-weighted image fails to depict the tumor owing to its relatively low signal intensity. The matrix size (126 × 126) was chosen erroneously. **(e–g)** Dynamic subtracted TurboFLASH images show early and rapid enhancement of the tumor. There is also some enhancement outside the contour of the prostate (arrow). This was interpreted as capsular perforation by one reader. Information obtained from time–signal intensity curves showed that this area enhanced earlier but the increase in signal intensity was less than that of the tumor. **(h)** Gross pathologic specimen shows small poorly differentiated tumor on the left side (red); there was no capsular perforation.

tal coil (MRInnervu; Medrad, Pittsburgh, Pa). The coil was inserted with the patient in the lateral decubitus position and inflated with 50–100 cm^3 of air. Peristalsis was suppressed by means of intravenous administration of 1 mg of glucagon. A tight band was wrapped around the patient's abdomen to decrease respiratory movement.

First, a sagittal T1-weighted localizing image was obtained to confirm the position of the coil and to select locations for the axial images. Axial T1-weighted images (420/22 [repetition time msec/echo time msec], two signals acquired) as well as axial, sagittal, and coronal fast spin-echo (SE) T2-weighted images (2,940/160, echo train length of 13, three signals acquired) were obtained. All examinations were performed with a 4- or 5-mm section thickness, a 0.8–1.5-mm gap, a 26-cm field of view, and a 512 × 216 matrix. An equalizing processing with application of a filter algorithm to compensate for near-field effect was used. We interchanged the direction of the phase-encoding gradient and the read-out gradient to decrease motion artifacts over the prostate.

The section for the gadolinium-enhanced MR images was selected from the T2-weighted axial fast SE images. A section was chosen in which tumor and normal prostatic tissue were likely to be present. When no tumor was visible, a level that demonstrated normal anatomic details or benign prostatic hyperplasia (BPH) was chosen. As the study proceeded, we preferably studied a section in which capsular penetration was not obvious. In this section during intravenous bolus injection of 0.1 mmol of gadopentetate dimeglumine (Magnevist; Schering, Berlin, Germany) per kilogram of body weight, 63 images were obtained by using a single-section TurboFLASH magnetization-prepared sequence (7/3/15 [repetition time msec/echo time msec/inversion time msec], 10° flip angle, 128 × 256 matrix, 200-mm field of view, 1-cm section thickness) with a speed of one image per 2.5 seconds in 15 patients (two signals acquired) and a speed of one image per 1.25 seconds in the other 42 patients (one signal acquired). Finally, multisection, axial, late-phase, postcontrast T1-weighted SE images (420/22, two signals acquired) were obtained. The examinations was performed by using a 4- or 5-mm section thickness, a 0.8–1.5-mm gap, a 26-cm field of view, and a 512 × 216 matrix.

The dynamic single-section images were transferred to a diagnostic workstation (Hewlett-Packard, Palo Alto, Calif). In our department, a computer program was developed to subtract the TurboFLASH images and to calculate color-coded time and slope images and maximal signal intensity images (Fig 1) (11,12). For the time images, the beginning of enhancement of prostatic tissue in relation to the beginning of arterial enhancement was color coded and projected over the unenhanced image. The beginning of enhancement was defined as an increase of 10 arbitrary units above the base noise line. For the positive slope image, the slope of maximal signal intensity increase was color coded. For the negative slope images (washout), the slope of signal intensity decrease, after maximal signal intensity, was color coded. The maximal signal intensity images display maximal enhancement 45 seconds after the beginning of arterial enhancement. Time–signal intensity curves were made in operator-defined regions of interest to determine enhancement patterns of iliac vessels and benign and malignant prostatic tissue. (Note: The subtraction technique is commercially available on most MR systems. The software program for time, slope, and maximal signal intensity images is available from the authors on request.)

MR Image Evaluation

The T2-weighted fast SE images, the T1-weighted postcontrast images, and the subtracted images were interpreted independently by two observers (G.J.J., J.O.B.) who were blinded to the clinical findings and laboratory and imaging results.

The T2-weighted, postcontrast T1-weighted, and dynamic subtracted TurboFLASH images were interpreted for presence and location of tumor and capsular penetration by tumor. At the level of the dynamic subtracted TurboFLASH images, the prostate was divided into four areas: peripheral zone left and right and central zone left and right. The presence of tumor was scored on a five-point scale: 1 = definitely absent, 2 = probably absent, 3 =

a.

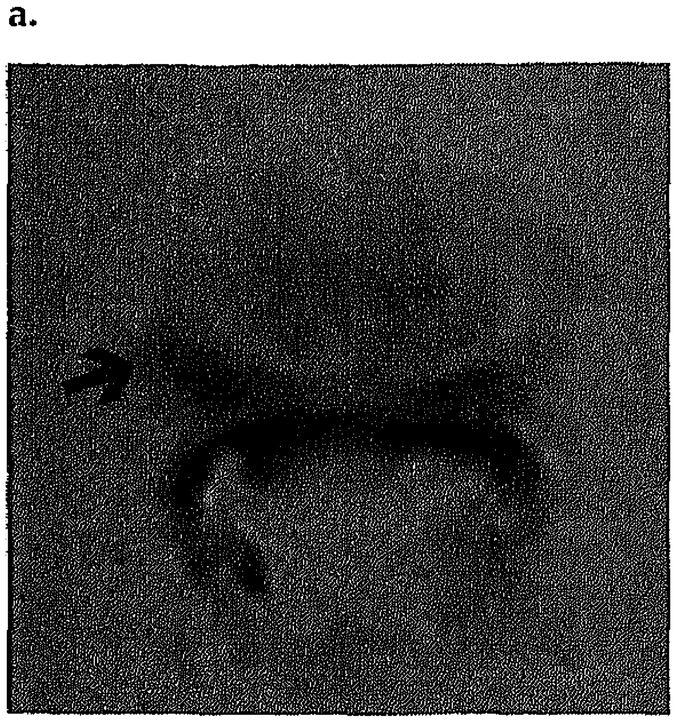

b.

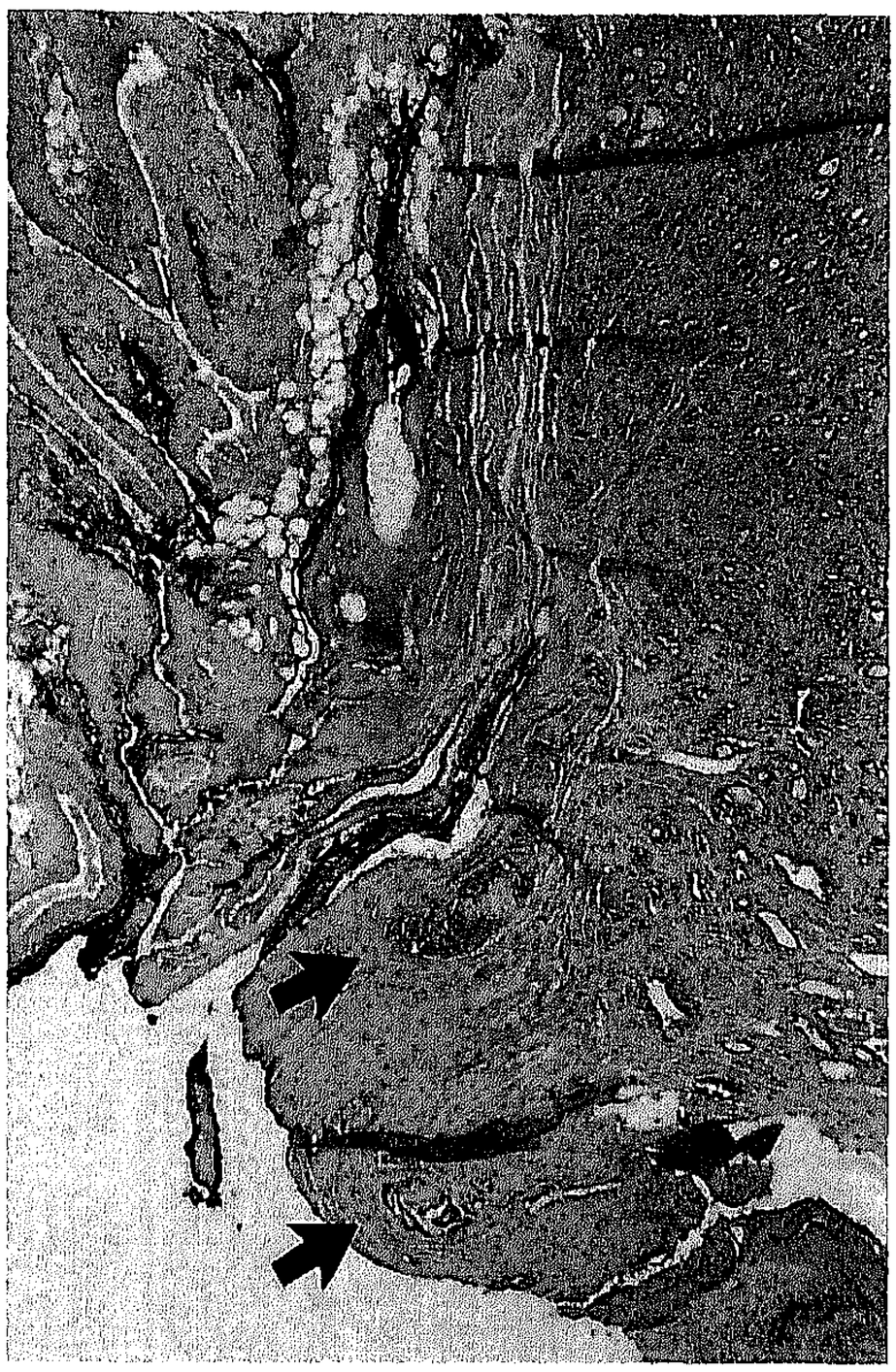

c.

Figure 2. Case of a 63-year-old-man with tumor involvement on the right side. (a) T2-weighted fast SE image shows retraction of the capsule on the right side (arrow) that was not interpreted as capsular penetration. (b) Dynamic subtracted TurboFLASH image shows enhancement outside the contour of the prostate (arrow) interpreted as capsular perforation. Capsular perforation was present at final pathologic examination. (c) Histopathologic specimen at the level of the right neurovascular bundle shows that, at the dorsolateral side, tumor is present and growing outside the prostatic capsule (pT3a, in which p = pathologic classification and a = unilateral capsular extension) (arrows). (Hematoxylin-eosin stain; original magnification, ×20.)

indeterminate, 4 = probably present, 5 = definitely present. Capsular penetration was scored on a three-point scale: 1 = no, 2 = indeterminate, 3 = yes. Regions representing cancer were outlined in a diagram. The area of tumor involvement for each lesion was determined by using the ellipsoid formula, and the total area of cancer involvement was calculated as the sum of cancer areas on the selected section.

On T2-weighted images, an area in the peripheral zone with relatively low signal intensity was considered to represent malignancy. Low-signal-intensity areas in the central zone were not interpreted as being malignant; however, when an obvious malignant peripheral lesion extended into the central zone, this was interpreted as positive for central tumor involvement. If a low-signal-intensity area showed high signal intensity on the corresponding T1-weighted image, the area was considered to be hematoma. The criteria for capsular perforation were disruption of the prostatic capsule, infiltration of the periprostatic fat, low-signal-intensity stranding, and involvement of the neurovascular bundle. A bulge in the contour or capsular thickening was interpreted as "probable" (2 on the three-point scale) capsular perforation (13).

The onset and slope of enhancement were assessed on hard-copy images made of the subtraction set. The onset of enhancement of prostatic tissue in relation to the onset of arterial enhancement was registered in seconds. The slope of enhancement was scored on a three-point scale: 1 = slow, 2 = normal, 3 = fast.

On the subtracted images, a lesion was considered to represent malignancy if the slope of enhancement was faster and the onset was earlier relative to the adjacent prostatic tissue. Enhancement outside the contour of the prostate was considered to represent capsular penetration (Fig 2).

With use of these criteria, the additional value of the TurboFLASH technique was assessed.

Pathologic Examination

The prostatectomy specimens were fixed in toto overnight in a solution of 10% neutral buffered formalin. Step sections were made at 4-mm intervals in a plane parallel to the base of the prostate, which corresponded to the sections used for axial MR imaging. After separating the step sections into right and left halves, all sections were routinely embedded in paraffin. Tissue sections of 4 μm were prepared and stained with hematoxylin-eosin. Regions representing cancer were outlined on the glass cover and retraced onto a diagram of the axial histologic sections that extended from the base to the apex of the prostate. The area of tumor involvement for each lesion was determined by using the ellipsoid formula, and the total area of cancer involvement was calculated as the sum of cancer areas on the selected section. Measurements were multiplied by a factor of 1.1 to correct for tissue shrinkage due to fixation.

Data Analysis

Analysis of the correlation of MR findings and histopathologic results was performed by two radiologists (G.J.J., J.O.B.) and one pathologist (E.T.G.R). The MR images were correlated with tumor maps on the basis of the histopathologic sections. The level of the dynamic subtracted TurboFLASH images was determined by its location between the apex and base of the prostate. The corresponding pathologic slice of the tumor map was then adjusted. Because of the difference between section thickness of the TurboFLASH images (10 mm) compared with that of the fast SE images (4 mm) and the gross specimen (4 mm), tumor maps of adjacent pathologic slices were also considered.

Penetration through the capsule was compared for each quadrant.

Statistical Analysis

The McNemar test (exact distribution) was used to evaluate the differences in assessing tumor presence and capsular penetration with both techniques.

Cohen κ analysis was used to test for agreement between both readers with respect to the presence and absence of tumor and capsular penetration: $\kappa < 0.40$, poor agreement; $\kappa = 0.4$–0.75, good agreement; $\kappa > 0.75$, strong agreement.

When sensitivity and specificity values for tumor presence were calculated, scores 4 and 5 were considered "present." When sensitivity and specificity values for capsular penetration were calculated, score 3 was considered "present."

Additional Diagnostic Value

The overall additional diagnostic value of dynamic subtracted TurboFLASH images to routine MR imaging was determined as follows: Major improvement of the diagnostic performance was present when dynamic subtracted TurboFLASH images allowed correct overstaging (T2→T3) or understaging (T3→T2), minor improvement was present when the estimated area of tumor involvement as determined on the dynamic subtracted TurboFLASH images came within the 25% range of the actual tumor (Figs 3, 4). Diagnostic performance was defined as "worse staging" when over- or understaging was incorrect with dynamic subtracted TurboFLASH images and "worse (minor)" when the estimated

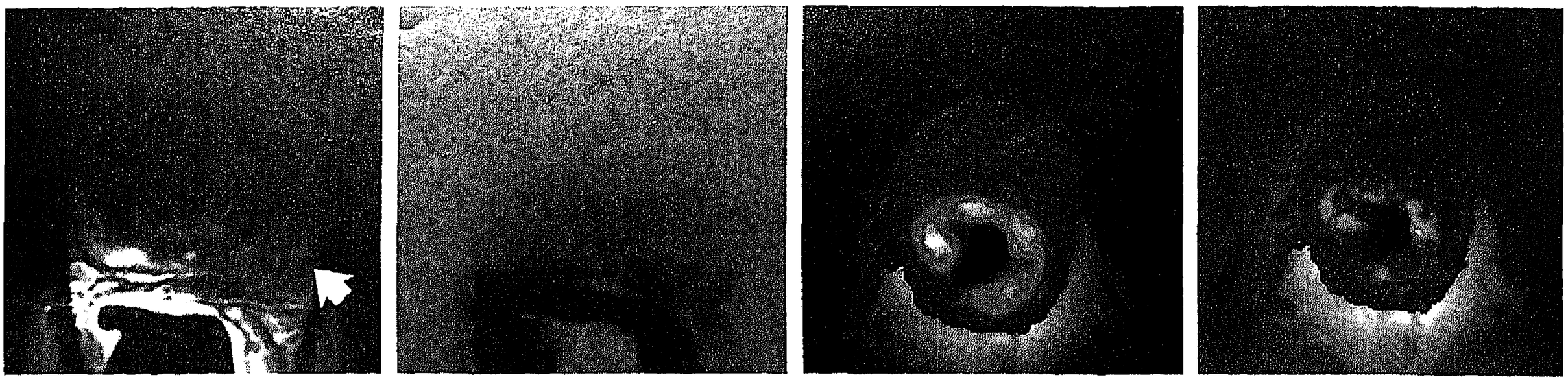

a. b. c. d.

Figure 3. Case of a 66-year-old man with prostate cancer. **(a)** T2-weighted fast SE image shows a low-signal-intensity area on the left side and bulging of the contour (arrow). This was interpreted as a T2 tumor by one observer and a T3 tumor by the other. **(b)** Dynamic subtracted TurboFLASH image shows little enhancement. **(c)** Time image shows late enhancement, and **(d)** slope image shows slow enhancement. No tumor was found at the corresponding level at final pathologic examination.

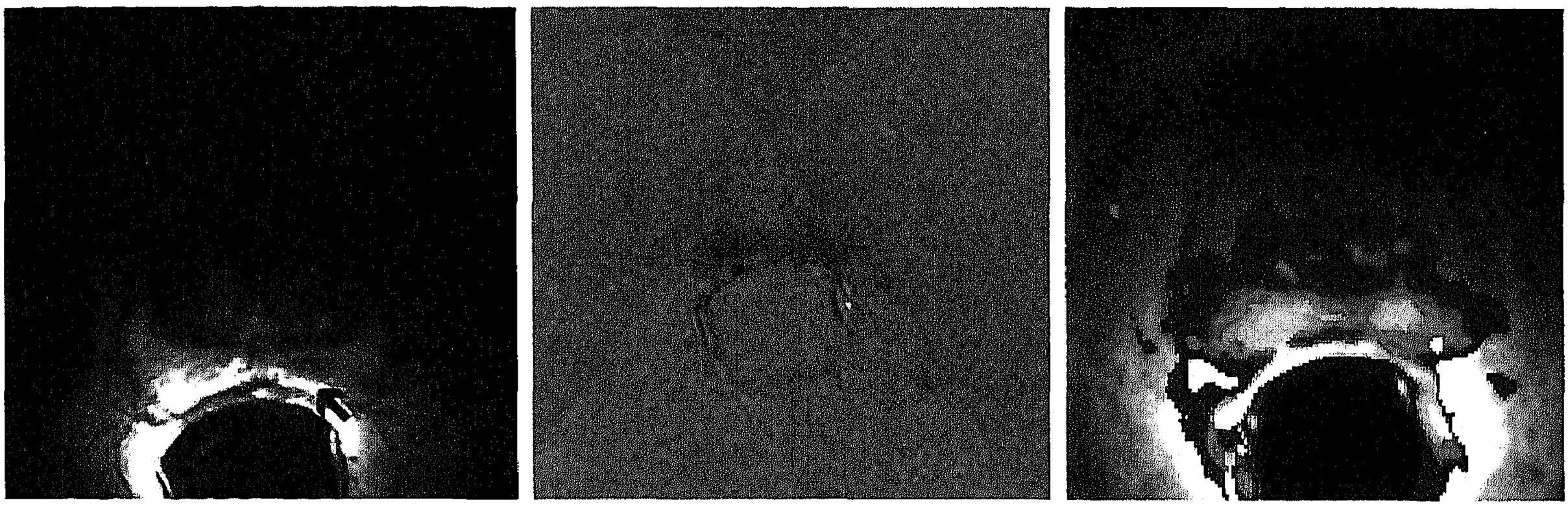

a. b. c. d.

Figure 4. Case of a 57-year-old man with prostate cancer. **(a)** T2-weighted fast SE image shows a small area of low signal intensity on the left side (arrow). **(b)** Dynamic subtracted TurboFLASH and **(c)** time images show symmetrically early and rapid enhancement of the peripheral zone. **(d)** Photomicrograph shows moderately differentiated tumor. This tumor was present on both sides and correlated with the area of enhancement. (Hematoxylin-eosin stain; original magnification, ×20.)

area of tumor involvement as determined on the dynamic subtracted TurboFLASH images exceeded the 25% range of the actual tumor area correlated with the corresponding step-section histologic slice (Fig 5). Additional information of dynamic subtracted TurboFLASH images that did not change the final staging result was called "minor." For example, dynamic subtracted TurboFLASH images depicted capsular penetration not depicted on fast SE images, but fast SE images had already depicted seminal vesicle invasion (T3c).

RESULTS

Correlating MR and Histopathologic Findings

The correlation between MR images and the corresponding histopathologic section was difficult in most patients. The most caudal section of the MR images was 0.5–1.5 cm more distal than the most apical section of the prostatectomy specimen. Also, the angle by which the sections were cut in both techniques was never exactly the same for either technique (difference, 5°–15°). Furthermore, the shape of the prostate changed after surgery and fixation compared with the shape of the gland within the body at the time of imaging. Also making correlation difficult was the fact that prostate tumors are very irregular and often demonstrate fingerlike projections with ill-defined margins, which did not display on MR images of 4-, 5-, or 10-mm section thickness (whereas the histologic sections were only 4 μm thick). We tried to overcome these problems by using tumor maps, which gave a good three-dimensional picture of the prostate and were of help in assessing the corresponding level.

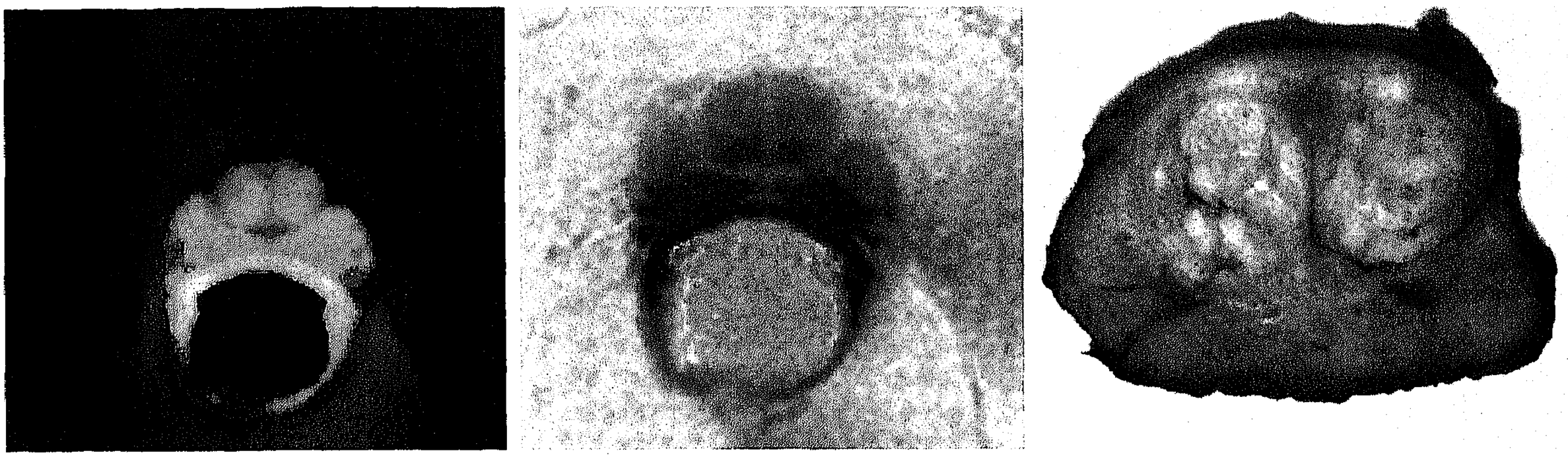

a. b. c.

Figure 5. Case of a 52-year-old man with a very small focus of prostate cancer (0.4 cm^3). (a) Time and (b) maximal signal intensity images show symmetrically rapid and early enhancement. (c) Gross specimen of the corresponding section shows BPH. No tumor was present at the corresponding level.

Table 1
Sensitivity and Specificity for Tumor Localization with Fast SE and Dynamic Subtracted TurboFLASH Imaging

Zone	Fast SE		TurboFLASH	
	Reader 1	Reader 2	Reader 1	Reader 2
	Sensitivity			
Tumor present				
Peripheral ($n = 72$)	53 (74)	55 (76)	58 (81)	60 (83)
Central ($n = 30$)	5 (17)	4 (13)	17 (57)	14 (47)
Total ($n = 102$)	58 (57)	59 (58)	75 (74)	74 (72)
	Specificity			
Tumor absent				
Peripheral ($n = 42$)	27 (64)	22 (52)	24 (57)	31 (74)
Central ($n = 84$)	82 (98)	81 (96)	76 (90)	73 (87)
Total ($n = 126$)	99 (79)	103 (82)	100 (79)	104 (82)

Note.—Numbers in parentheses are percentages.

Characterization of Enhancement Patterns

Differences in enhancement within the prostate were best depicted in the early phase of the first pass of contrast material. However, most glandular tissue of the prostate displayed early enhancement, and there was a considerable variation between the start of enhancement of the external iliac artery (t = 0) and the start of enhancement of prostatic tissue. Therefore, the onset of enhancement was judged relative to the adjacent prostatic tissue. We were also not able to characterize the time–signal intensity curve (slope of enhancement) for malignant or benign lesions. Therefore, relative differences in slope values in the selected section were used to differentiate between benign and malignant lesions.

Interobserver Agreement

Interobserver agreement for the interpretation of MR images with and without the dynamic subtracted TurboFLASH sequence was strong. The Cohen κ values were 0.79 and 0.78, respectively.

Both observers agreed that nondynamic T1-weighted postcontrast images did not provide additional information compared with T2-weighted fast SE images.

Detection of Tumor

A total of 228 quadrants were identified, rated, and analyzed. Tumor was present in 102 quadrants. The results for predicting tumor presence with and without dynamic subtracted TurboFLASH images are presented in Table 1. For each reader, the sensitivity for detection of tumor with fast SE images was 57% and 58%, respectively, and with dynamic subtracted TurboFLASH images was 74% and 73%, respectively (the differences between sequences were not statistically significant). The specificity for fast SE images was 79% and 82% and for dynamic subtracted TurboFLASH images was 79% and 83%, per reader respectively (the differences between sequences were not statistically significant). The accuracy for fast SE images was 73% and 71% and for dynamic subtracted TurboFLASH images was 77% and 78% (the differences between sequences were not statistically significant).

Tumor Volume

In 17 (30%) and 18 (32%) of the 57 patients, the area of tumor involvement estimated with fast SE images was within the 25% range of the actual area of tumor involvement, per reader respectively. With dynamic subtracted TurboFLASH images, the estimated tumor volume was within the 25% range in 23 (40%) and 25 (44%) patients (the differences between sequences were not statistically significant).

Capsular Penetration

Two hunderd twenty-eight quadrants were evaluated. Capsular penetration was present at histopathologic examination in 19 different quadrants, in 14 patients. In the remaining 209 quadrants, capsular penetration was absent, including one site where capsular penetration could not be evaluated because the surgeon incised the capsule. With fast SE images, the readers correctly diagnosed capsular penetration in four and three quadrants, respectively. False-positive diagnoses were made at two sites. With dynamic subtracted TurboFLASH images, the readers correctly diagnosed capsular penetration in nine and 10 quadrants, respectively. With dynamic subtracted TurboFLASH images, false-positive diag-

noses were made in one and two quadrants, per reader respectively. When considering both sequences, capsular penetration was predicted more accurately with dynamic subtracted TurboFLASH images by both readers in six and nine quadrants in six (11%) and nine (16%) patients, respectively, but less accurately in zero and two quadrants in zero and two (4%) patients (the differences between sequences was not statistically significant). Three other patients, in whom the findings were true-negative for capsular penetration, had capsular penetration at a different level than that of the dynamic subtracted TurboFLASH images. Capsular penetration was depicted in one of these three on fast SE images.

Additional Diagnostic Value

The additional diagnostic value of dynamic subtracted TurboFLASH images to routine MR imaging is summarized in Table 2. We achieved overall major improvement in five and seven patients, per reader respectively, and overall minor improvement in eight and six patients, respectively.

DISCUSSION

The merit of MR imaging is in the local staging of prostate cancer. Although microscopic capsular penetration may not be demonstrated on T2-weighted images, MR imaging may be helpful in selecting patients with a potentially resectable disease (13,14). More accurate staging, however, is needed.

Several studies have addressed the use of contrast material in MR imaging of the prostate (5–10,15). In the normal prostate, the central zone enhances more than the peripheral zone. Both enhance homogeneously. In the presence of BPH, the enhancement pattern of the central gland is markedly inhomogeneous (6,8). BPH may occasionally arise within the peripheral zone of the prostate, leading to an inhomogeneous enhancement.

Prostate cancer is frequently reported to show increased enhancement compared with that of adjacent glandular tissue, especially in the peripheral zone; in the central zone, the difference is less obvious (8).

Reported studies suggest that contrast enhancement in prostate cancer is of limited value and may be only helpful in cases of seminal vesicle invasion (6,15).

Brown et al (8) evaluated bolus-enhanced MR imaging in prostate carcinoma. They showed that early-phase contrast-enhanced images best enabled the definition of tumor within the gland in 10 (50%) of 20 patients and demonstrated capsular spread more clearly in eight (80%) of the 10 patients. In that study, no pathologic correlation could be obtained.

Malignant breast, bladder, and bone tissues have demonstrated early and fast enhancement. The enhancement pattern can be characterized by the onset of enhancement (11,16) or by the slope of enhancement (17). We evaluated the enhancement of prostate cancer during the first pass of contrast material with fast dynamic imaging with a temporal resolution of one image per 1.2 or 2.24 seconds after bolus administration of intravenous contrast material. Our findings indicate that prostate cancer also enhances early and that differences in enhancement are visible in the early phase of the first pass. However, owing to a large variation in the onset and slope of enhancement among the patients in our study and minor differences between the onset of enhancement of carcinoma and benign tissue, which bring about a considerable overlap between benign and malignant lesions in quantitative measures, we were not able to define a cutoff time nor a slope value to differentiate benign from malignant prostatic tissue. Therefore, the onset and slope of enhancement were judged relative to adjacent prostatic tissue.

Because we used subjective signs, independent double reading was performed to test for interobserver variability. There appeared to be strong agreement between both readers for the interpretation of both fast SE and dynamic subtracted TurboFLASH images. This is contrary to other studies, which have reported high interobserver variation in estimating tumor location, tumor volume, and capsular penetration of the prostate (18,19). The high agreement of our readers may be due to the study design. The section of the dynamic subtracted TurboFLASH images was chosen in a plane that was likely to contain both cancer and normal tissue on the T2-weighted fast SE image.

Reported data for detection of tumors with MR imaging are, in general, poor especially for central gland tumors (20,21). The sensitivity for localization of tumors with dynamic subtracted TurboFLASH imaging was consistently better than that with fast SE images. It was confirmed that tumors located ventrally and centrally in histopathologic specimens were easily missed on T2-weighted images. With dynamic subtracted TurboFLASH imaging, there were 12 and 10 more true-positive centrally located tumors than that with SE imaging but also six and eight more false-positive tumors.

Table 2
Additional Diagnostic Value of Dynamic Subtracted TurboFLASH Images

Diagnostic Performance with TurboFLASH	Reader 1	Reader 2
Improved staging	5	8
Better (minor)	13	12
Equal	34	30
Worse (minor)	5	6
Worse staging	0	1

Note.—Data are numbers of patients.

Tumor volume is a predictor of pathologic stage (22). Except for one study performed with an external-array coil (23), studies performed with endorectal coil (13) and body coil MR imaging (24–27) reported a poor correlation between MR tumor volume and the volume as calculated from the pathologic specimen. Mirowitz et al (6) who studied postcontrast T1-weighted images also reported poor correlation between the estimated and calculated volume. Brown et al (8) found better correlation during the early phase of enhancement, but in that study pathologic confirmation was not obtained.

When compared with fast SE images, dynamic subtracted TurboFLASH images enabled better estimation of the area of tumor involvement in 10%–12% of the patients. However, in only 30%–32% of patients, the area of tumor involvement estimated with fast SE images was within the 25% range of the actual area of tumor involvement. One reason for overestimating tumor volume on dynamic subtracted TurboFLASH images was rapid enhancement of an area of BPH in the central zone (Fig 5). This error can be averted when symmetrically central enhancement is not considered as cancer.

In an overview, Schiebler et al (1) stated that body coil MR imaging gives unsatisfactory results in the detection of capsular penetration. The detection of capsular penetration improved with endorectal coil MR imaging (sensitivity, 67%) compared with body coil MR imaging (sensitivity, 44%) in the same patient cohort (28).

Results of recent studies with endorectal coil MR imaging, however, showed a limited accuracy to 33% for detection of capsular penetration (5,13,19,29,30).

In the present study, the sensitivity for detection of capsular penetration was 21% and 16% with fast SE, and 47% and 53% with dynamic subtracted TurboFLASH, per reader respectively. These values appeared not to be statistically significant. The low sensitivity for detection of capsular penetration with fast SE is because, at least in part, we only studied one level, preferably in which capsular penetration was not obvious. False-positive results on dynamic subtracted TurboFLASH images may be due to enhancement of a capsular artery. The vessel may be differentiated from tumor by a different enhancement curve (Fig 1).

Better prediction of capsular penetration is of clinical relevance because pathologic stage is the most important prognostic factor. Staging results improved because of a more accurate assessment of the capsule with dynamic subtracted TurboFLASH (Table 2).

T2-weighted MR images do not provide information about tumor grade, another predictor of clinical outcome. A noteworthy finding of the present study was that dynamic subtracted TurboFLASH images depicted all poorly differentiated tumors and that five of them showed the earliest and fastest enhancement of all lesions. These numbers are, however, too small for statistical analysis, and our study was not designed to differentiate between low-grade and high-grade lesions. These preliminary findings seem to be in contradiction with the findings of Yoshizako et al (9), who reported that poorly differentiated tumors demonstrate less enhancement on contrast-enhanced T1-weighted images than that of moderately differentiated tumors. However, we also observed that rapidly enhancing tumors demonstrated relatively low signal intensity on late-phase postcontrast images (Fig 1d), which may be explained by the high washout of contrast material from the tumor (Fig 1c).

Our study shows that the results of MR imaging with the dynamic subtracted TurboFLASH sequence were consistently better than those of routine MR imaging, although routine use of single-section dynamic subtracted TurboFLASH images did not statistically significantly improve tumor localization and staging results. The results of dynamic subtracted TurboFLASH imaging may, however, be improved. First, there was a learning curve. Second, a number of examinations were carried out in patients in whom the clinical stage was obvious from fast SE images. In these cases, dynamic subtracted TurboFLASH images did not provide additional information.

More limitations were inherent to the TurboFLASH technique we used; the single-section imaging technique allows evaluation in only one plane. Capsular penetration may be present at another level. Better delineation of tumor and tumor volume may become possible when with echo-planar imaging a dynamic multisection technique can be performed with a time resolution of a minimum of 3 seconds. Also, the spatial resolution is considerably less than with fast SE images, and the section is twice as thick. Another limiting factor of our technique was the endorectal coil–dependent variation of signal intensity throughout the prostate gland. Especially, lesions located ventrally are difficult to recognize because they show relatively less enhancement. In addition, the rectum-prostate interface is full of enhancement-like artifacts. In our series, better staging occurred predominantly at the dorsolateral side. The assessment at the dorsal side was difficult. Easily applicable corrections for the coil profile may be helpful. These problems may be overcome with the introduction of a combined endorectal–phased array coil, which will provide a more homogeneous signal through the prostate, a higher signal-to-noise ratio, and a decreased reliance on filters. Another limitation of the dynamic subtracted TurboFLASH technique is that onset and slope of enhancement of benign and malignant tissue show some overlap; therefore, false-positive and false-negative results may occur.

In conclusion, we demonstrated that prostate cancer shows early and rapid enhancement and that with fast imaging and the use of a subtraction technique tumor assessment may be improved. However, routine use of the single-section method did not statistically significantly improve staging results. Further improvement of the technique may be achieved by application of a multisection sequence, by the introduction of a combined endorectal–phased array coil, and by correction for the sensitivity profile of the endorectal coil throughout the prostate gland. ■

Acknowledgment: The authors thank Howard M. Pollack, MD, for his review of the manuscript and helpful suggestions.

References

1. Schiebler ML, Schnall MD, Pollack HM, et al. Current role of MR imaging in the staging of adenocarcinoma of the prostate. Radiology 1993; 189:339–352.
2. Denis LJ, Murphy GP, Schroeder FH. Report of the consensus workshop on screening and global strategy for prostate cancer. Cancer 1995; 75:1187–1207.
3. Perrotti M, Kaufman RP Jr, Jennings TA, et al. Endo-rectal coil magnetic resonance imaging in clinically localized prostate cancer: is it accurate? J Urol 1996; 156:106–109.
4. Bostwick DG, Qian J, Bergstralh EJ, et al. Prediction of capsular perforation and seminal vesicle invasion in prostate cancer. J Urol 1996; 155:1361–1367.
5. Quinn SF, Franzini DA, Demlow TA, et al. MR imaging of prostate cancer with an endorectal surface coil technique: correlation with whole-mount specimens. Radiology 1994; 190:323–327.
6. Mirowitz SA, Brown JJ, Heiken JP. Evaluation of the prostate and prostatic carcinoma with gadolinium-enhanced endorectal coil MR imaging. Radiology 1993; 186:153–157.
7. Sommer FG, Nghiem HV, Herfkens R, McNeal JE. Gadolinium-enhanced MRI of the abnormal prostate. Magn Reson Imaging 1993; 11:941–948.
8. Brown G, Macvicar DA, Ayton V, Husband JE. The role of intravenous contrast enhancement in magnetic resonance imaging of prostatic carcinoma. Clin Radiol 1995; 50:601–606.
9. Yoshizako T, Sugimura K, Kaji Y, Moriyama M, Wada A. Prostate and prostatic carcinoma: comparison of gadolinium-enhanced MR images and histopathologic findings. Nipon Igaku Hoshasen Gakkai Zasshi 1995; 55:545-549. [Japanese]
10. Huch Böni RA, Boner JA, Lütolf UM, Trinkler F, Pestalozzi DM, Krestin GP. Contrast-enhanced endorectal coil MRI in local staging of prostate carcinoma. J Comput Assist Tomogr 1995; 19:232–237.
11. Boetes C, Barentsz JO, Mus RD, et al. MR characterization of suspicious breast lesions with gadolinium-enhanced TurboFLASH subtraction technique. Radiology 1994; 193:777–781.
12. Barentsz JO, Jager GJ, van Vierzen PBJ, et al. Staging urinary bladder cancer after transurethral biopsy: the value of fast dynamic contrast-enhanced MR imaging. Radiology 1996; 201:185–193.
13. Jager GJ, Ruijter ETG, van de Kaa CA, et al. Local staging of prostate cancer with endorectal MR imaging: correlation with histopathology. AJR 1996; 166:845–852.
14. d'Amico AV, Whittington R, Schnall MD, et al. The impact of the inclusion of endorectal coil magnetic resonance imaging in a multivariate analysis to predict clinically unsuspected extraprostatic cancer. Cancer 1995; 75:2368–2372.
15. Huch Böni RA, Boner JA, Debatin JF, et al. Optimization of prostate carcinoma staging: comparison of imaging and clinical methods. Clin Radiol 1995; 50:593–600.
16. Schnall MD, Bezzi M, Pollack HM, Kressel HY. Magnetic resonance imaging of the prostate. Magn Res Q 1990; 6:1–16.
17. Verstraete KL, De Deene Y, Roels H, Dierick A, Uyttendaele D, Kunnen M. Benign and malignant musculoskeletal lesions: dynamic contrast-enhanced MR imaging—parametric "first-pass" images depict tissue vascularization and perfusion. Radiology 1994; 192:835–843.
18. Schiebler ML, Yankaskas BC, Tempany CMC, et al. MR imaging in adenocarcinoma of the prostate: interobserver variation and efficacy for determining stage C disease. AJR 1992; 158:559–562.

19. Tempany CMC, Zhou X, Zerhouni EA, et al. Staging of prostate cancer: results of radiology diagnostic oncology group project comparison of three MR imaging techniques. Radiology 1994; 192:47–54.
20. Carter HB, Brem RF, Tempany CMC, et al. Nonpalpable prostate cancer: detection with MR imaging. Radiology 1991; 178: 523–525.
21. Lovett K, Rifkin MD, McCue PA, Choi H. MR imaging characteristics of noncancerous lesions of the prostate. JMRI 1992; 2:35–39.
22. Bryan PJ, Butler HE, Li Puma JP. NMR scanning of the pelvis: initial experience with a 0.3 tesla system. AJR 1983; 141: 1111–1118.
23. Sommer FG, Nghiem HV, Herfkens R, McNeal JE, Low RN. Determining the volume of prostatic carcinoma: value of MR imaging with an external-array coil. AJR 1993; 161:81–86.
24. Bezzi M, Kressel HY, Allen KS, et al. Prostatic carcinoma: staging with MR imaging at 1.5 T. Radiology 1988; 169:339–346.
25. Kahn T, Bürrig K, Schmitz-Drager B, Lewin JS, Fürst G, Modder U. Prostatic carcinoma and benign prostatic hyperplasia: MR imaging with histopathologic correlation. Radiology 1989; 173:847–851.
26. McSherry SA, Levy F, Schiebler ML, Keefe B, Dent GA, Mohler JL. Preoperative prediction of pathological tumor volume and stage in clinically localized prostate cancer: comparison of digital rectal examination, transrectal ultrasonography and magnetic resonance imaging. J Urol 1991; 146:85–89.
27. Quint LE, Van Erp JS, Bland PH, et al. Carcinoma of the prostate: MR images obtained with body coils do not accurately reflect tumor volume. AJR 1991; 156:511–516.
28. Schnall MD, Imai Y, Tomaszewski JE, Pollack HM, Lenkinski RE, Kressel HY. Prostate cancer: local staging with endorectal surface coil MR imaging. Radiology 1991; 178:797–802.
29. Chelsky MJ, Schnall MD, Seidmon EJ, Pollack HM. Use of endorectal surface coil magnetic resonance imaging for local staging of prostate cancer. J Urol 1993; 150:391–395.
30. Outwater E, Petersen RO, Siegelman ES, Gomella LG, Chernesky CE, Mitchell DG. Prostate carcinoma: assessment of diagnostic criteria for capsular penetration on endorectal coil MR images. Radiology 1994; 193:333–339.